NANO LETTERS

pubs.acs.org/NanoLett

Letter

# Superconducting Cavity-Based Sensing of Band Gaps in 2D Materials

Krishnendu Maji, Joydip Sarkar, Supriya Mandal, Sriram H., Mahesh Hingankar, Ayshi Mukherjee, Soumyajit Samal, Anirban Bhattacharjee, Meghan P. Patankar, Kenji Watanabe, Takashi Taniguchi, and Mandar M. Deshmukh*

Cite This: *Nano Lett.* 2024, 24, 4369−4375

Read Online

ACCESS | Metrics & More | Article Recommendations | Supporting Information

**ABSTRACT:** The superconducting coplanar waveguide (SCPW) cavity plays an essential role in various areas like superconducting qubits, parametric amplifiers, radiation detectors, and studying magnon-photon and photon-phonon coupling. Despite its wide-ranging applications, the use of SCPW cavities to study various van der Waals 2D materials has been relatively unexplored. The resonant modes of the SCPW cavity exquisitely sense the dielectric environment. In this work, we measure the charge compressibility of bilayer graphene coupled to a half-wavelength SCPW cavity. Our approach provides a means to detect subtle changes in the capacitance of the bilayer graphene heterostructure, which depends on the compressibility of bilayer graphene, manifesting as shifts in the resonant frequency of the cavity. This method holds promise for exploring a wide class of van der Waals 2D materials, including transition metal dichalcogenides (TMDs) and their moiré, where DC transport measurement is challenging.

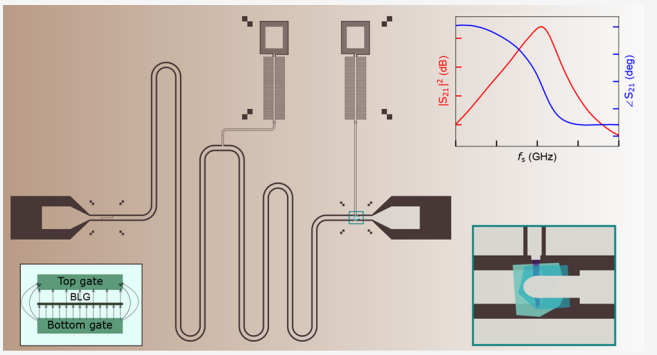


**KEYWORDS:** *superconducting cavity, 2D materials, bilayer graphene, microwave, capacitance*



Superconducting coplanar waveguide (SCPW) cavities are structures designed to confine and manipulate electromagnetic fields at microwave frequencies,[1] which are widely used in diverse areas like coupling to superconducting qubit for readout,[2−5] parametric amplifiers,[6,7] bolometers,[8,9] fast charge sensing of quantum dots,[10] studying the magnon−photon interaction in van der Waals magnets,[11,12] studying the interaction with a spin ensemble,[13−15] and studying nanomechanical devices.[16−18] The SCPW cavities when operated at a resonant frequency are very sensitive and find applications in detecting small changes in the electromagnetic field[19,20] and radiation.[21] Consequently, SCPW cavities offer powerful and sensitive tools for investigating the electronic properties of van der Waals materials.

van der Waals 2D materials consist of atomically thin layers stacked on top of each other through a weak van der Waals force. These materials exhibit extraordinary electronic, optical, and mechanical properties due to their reduced dimensionality. Furthermore, the stacking of various van der Waals materials at specific angles between layers gives rise to new functionalities and electronic properties.[22−25] While various measurements have been conducted to study these materials, most have focused on low-frequency DC transport measurements. One of the key limitations of the DC transport measurement is that it requires ohmic contact between the electrodes and 2D materials. There is a wide range of 2D materials in which establishing ohmic contact is challenging. The significant advantage of the microwave technique is that it enables contactless transport measurements, such as measuring the electrical conductivity of a 2D heterostructure through the transmission of a capacitively coupled cavity, without the need for physical contacts or electrodes that might disrupt the behavior of 2D materials. The microwave cavity-based techniques exploit the extreme sensitivity of the resonant frequency to the effective dielectric or magnetic environment, and the high quality factor of the cavity improves this sensitivity. Numerous studies have employed microwave techniques to analyze low-dimensional materials. These studies encompass diverse applications, including measuring the charge occupation of quantum dots,[26] assessing minute capacitance,[27] and measuring the impedance of low-dimensional materials,[28] exploring the microwave properties of

**Received:** December 18, 2023
**Revised:** February 19, 2024
**Accepted:** February 20, 2024
**Published:** February 23, 2024

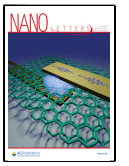





https://doi.org/10.1021/acs.nanolett.3c04990
*Nano Lett.* 2024, 24, 4369−4375

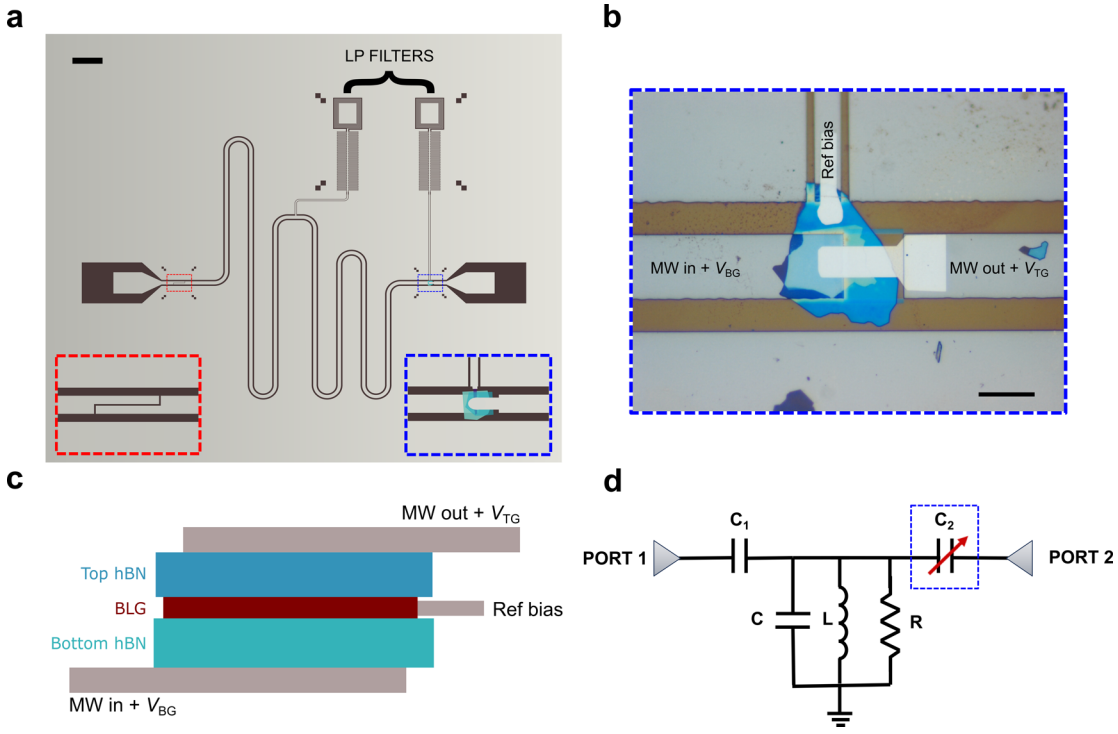


**Figure 1.** Coupling the 2D heterostructure to a superconducting cavity. (a) The representative schematic of the device. The $\lambda/2$ cavity is designed on a MoRe-sputtered $SiO_2$ (280 nm)/intrinsic Si (500 $\mu$m) substrate. The inset at the bottom left shows the finger coupling capacitor designed on the left side of the cavity. The inset on the bottom right side shows the zoomed-in image of the BLG heterostructure which serves as the second coupling capacitor $C_2$. The scale bar on the top left is 200 $\mu$m. (b) The optical image of the BLG heterostructure. The microwave (MW) signal and applied DC voltage schemes are indicated in the figure. The scale bar is 20 $\mu$m. (c) The cross-sectional schematic of the BLG heterostructure. (d) Schematic diagram of the equivalent circuit. The BLG stack plays the role of coupling capacitor $C_2$ marked by the blue dashed box.

graphene-based Josephson junction and their potential applications.[9,29−36]

In our work, we show an effective application of SCPW cavities to explore electronic compressibility, a parameter related to the density of states (DOS) in bilayer graphene (BLG). The BLG heterostructure is used as one of the coupling capacitors of a half-wave ($\lambda/2$) cavity with the ability to apply gate voltages to tune its band structure.[37] Specifically, we extracted the capacitance of the BLG stack from the transmitted signal through the cavity, where the resonant frequency shifts with the capacitance of the stack. This capacitance measurement allows us to extract the compressibility of the BLG. Moreover, the dual gate geometry of the device allows independent control of the charge density ($n$) in the BLG and perpendicular displacement field ($D$). The displacement field tunes the band gap of the BLG, thus modifying its DOS. Our compressibility measurement can capture this small opening of the band gap. Our method could be useful in studying various other 2D materials, and bilayer graphene serves as a demonstrator for the study of materials with small tunable gaps in the electronic spectrum. Extending our work to other 2D heterostructures could offer a highly sensitive and nonintrusive means of investigation, further enhancing our understanding of various 2D materials' properties. Most of the existing techniques to measure the capacitance of low-dimensional materials rely on lumped element circuits operating within a few hundred kHz range.[38,39] Whereas, our SCPW cavity operates at a few GHz frequency. The choice of GHz frequency range allows scopes for fast dynamical measurements in a cavity-coupled system[10,13,40] and can be extended to 2D material platforms as well.[41] A theoretical study has recently been conducted on quantum geometry-originated capacitance in insulators;[42] measuring the capacitance of flat-band moiré systems could provide insights into the quantum geometry. In addition, the moiré platform has been proposed as a route toward the quantum simulation of correlated electronic states.[43] Our technique can be useful to probe many of these quantum simulators experimentally.

Figure 1a shows a schematic representation of the fabricated device. The device is fabricated on a $SiO_2$ (280 nm)/intrinsic Si (500 $\mu$m) substrate. The substrate is initially DC magnetron sputtered with 50 nm MoRe, a type-II superconductor. Following this, photolithography and reactive ion etching are used to pattern the $\lambda/2$ SCPW cavity on the substrate. The cavity is designed to have a resonant frequency of around 6 GHz and a characteristic impedance of 50 Ω. The cavity is coupled to the input and output ports via coupling capacitors for transmission measurements. A finger coupling capacitor of 3.4 fF is designed at the input side.[1] At the output side, the van der Waals heterostructure served as the coupling capacitor. In our work, the stack consists of a BLG flake encapsulated between a top hBN and a bottom hBN (see Supporting Information, section 1 for details). Figure 1b shows the optical image of the heterostructure. The cross-section of the heterostructure is schematically shown in Figure 1c. The bottom gate voltage is applied through a low-pass (LP) filter linked to the CPW's central conductor at the voltage node to minimize microwave loss.[44] A bias tee is used to apply the top gate voltage through the output microwave port (see Supporting Information, section 2 for measurement details). The BLG is biased to zero potential through another LP filter.


https://doi.org/10.1021/acs.nanolett.3c04990
Nano Lett. 2024, 24, 4369−4375

The ability to apply multiterminal DC voltages is an added advantage as many moiré heterostructures have a band structure that is widely tunable with displacement field. The equivalent circuit of the device is illustrated in Figure 1d, where the heterostructure plays the role of the tunable coupling capacitor $C_2$, which is marked by the blue dashed box.

The measurements are done in a dilution fridge at 20 mK. The device is loaded inside an aluminum puck to eliminate stray magnetic fields and create a better electromagnetic environment at the base temperature. The transmission coefficient $S_{21}$, the ratio of the transmitted signal to the input signal, is measured as a function of frequency using a vector network analyzer (VNA). The amplitude and phase of the transmission coefficient, $S_{21}$, is plotted in Figure 2 as a function of signal frequency at zero gate voltages. The $\pi$ phase change is a characteristic of the $\lambda/2$ cavity measured in the transmission mode. The resonant frequency of the cavity is around 5.152 GHz. In the Supporting Information, Figure S2, the COMSOL simulation result of the cavity is shown.

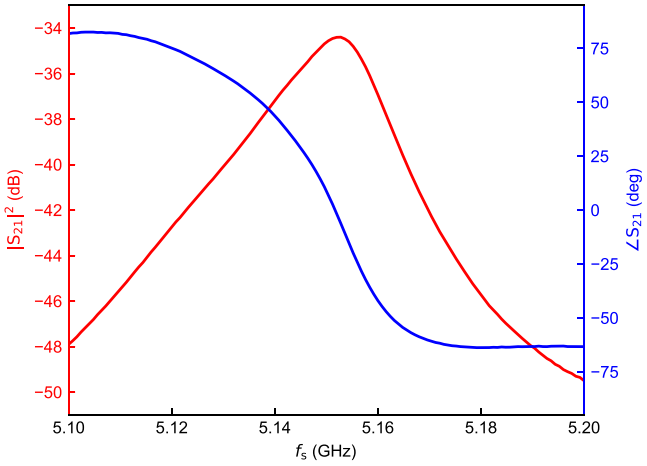


**Figure 2.** Cavity characterization. The red curve and the blue curve show the amplitude ($|S_{21}|^2$) and phase ($\angle S_{21}$) of the transmission coefficient, respectively, of the cavity at zero gate voltages. The resonant frequency is around 5.152 GHz. The cavity is showing a $\pi$ phase change at the resonance, which is the characteristic of a $\lambda/2$ cavity measured in transmission mode.

The device is fabricated in a dual-gate configuration, which enables independent control over the carrier density ($n$) of the BLG and the perpendicular displacement field ($D$) by adjusting both the top gate voltage ($V_{TG}$) and the bottom gate voltage ($V_{BG}$). In addition, the bilayer graphene is biased to 0 V to provide a ground reference for the DC electrostatic tuning of the system. In pristine BLG, the two graphene layers are electrically identical, making it an inversion-symmetric system. Consequently, there is no band gap in its electronic structure as shown in Figure 3b. Upon application of a perpendicular displacement field, an electrostatic potential difference is created between the two layers (shown in Figure 3a), breaking the inversion symmetry and resulting in the opening of a band gap (shown in Figure 3b).

There are two ways to probe the system experimentally. First, one measures the $S_{21}$ frequency response of the cavity-coupled device at each of the values of $V_{TG}$ and $V_{BG}$ creating a 4-dimensional data set, and second, by observing cavity response at a frequency close to the resonant mode of the system and varying the gate voltages creating a 3-dimensional data set. In this work, we focus on the first method of probing the system. For each ($V_{TG}$, $V_{BG}$), $S_{21}$ as a function of frequency is measured. Then the peak value of $|S_{21}|^2$ for each ($V_{TG}$, $V_{BG}$) is extracted from the data, which is plotted in Figure 3c. The data is also taken in the second way where the transmission signal is measured at a fixed frequency close to the resonance (Supporting Information, Figure S3). In our data, an offset of $V_{BGoffset} = -1.15$ V and $V_{TGoffset} = -2.7$ V is observed in $V_{BG}$ and $V_{TG}$, respectively, likely due to the charge doping in graphene from the metallic top and bottom gate which has been previously reported.[45] The data offer clearer physical insights if plotted in ($n$, $D$) space instead of ($V_{BG}$, $V_{TG}$). The transformation from ($V_{BG}$, $V_{TG}$) to ($n$, $D$) is achieved using the following set of equations: $n = (C_{BG}V'_{BG} + C_{TG}V'_{TG})/e$ and $D = (C_{BG}V'_{BG} - C_{TG}V'_{TG})/2$, where $C_{BG}$ ($C_{TG}$) is the capacitance of the bottom (top) gate, $V'_{BG}(V'_{TG}) = V_{BG}(V_{TG}) - V_{BGoffset}(V_{TGoffset})$ is the offset corrected bottom (top) gate voltage, and $e$ is the electronic charge. The plot in Figure 3c is transformed to the ($n$, $D/\epsilon_0$) plane from the ($V_{BG}$, $V_{TG}$) plane in Figure 3d. Only the positive displacement field sector data are shown here (see Supporting Information, Figure S4 for the full range data). A region with low transmission appears along the electric displacement field axis. This region corresponds to the opening of a band gap in the BLG caused by the perpendicular displacement field.[37] The width of the low transmission region at a particular displacement field relates to the band gap of the BLG at that displacement field. On looking closely at the data, one can see in the low transmission region two subfeatures emerge. These subfeatures correspond to two charge neutrality points and can be attributed to the spatial inhomogeneous doping in the device, a consequence of its larger overall area of ~30 $\mu m^2$. In the data shown in Figure 3c,d, a van-Hove singularity-like feature appears at the band edge of the BLG, which is a characteristic of BLG band structure (see Supporting Information, section 4.3 for details).

To extract the capacitance of the heterostructure, the data is fitted with the scattering coefficients $S_{21}$ of a capacitively coupled $\lambda/2$ CPW cavity, which can be written as[46]

$$S_{21} = \frac{2}{A + B/Z_0 + CZ_0 + D} + b \tag{1}$$

where $A$, $B$, $C$, and $D$ are the elements of the transmission matrix or ABCD matrix

$$A = \cosh(\gamma l) + \frac{\sinh(\gamma l)}{j\omega C_1 Z_0}$$

$$B = \sinh(\gamma l)\left(Z_0 - \frac{1}{\omega^2 C_1 C_2 Z_0}\right) + \cosh(\gamma l)\left(\frac{1}{j\omega C_1} + \frac{1}{j\omega C_2}\right)$$

$$C = \frac{\sinh(\gamma l)}{Z_0}$$

$$D = \cosh(\gamma l) + \frac{\sinh(\gamma l)}{j\omega C_2 Z_0}$$

where $l$ is the length of the transmission line, $\gamma = \alpha + j\beta$ is the complex propagation constant of the microwave field, $Z_0$ is the characteristic impedance of the transmission line. For $\lambda/2$ cavity $\beta l = \pi + \pi(\omega - \omega_0)/\omega_0$, where $\omega_0$ is the bare resonant frequency and $\alpha l = \pi/(2Q_i)$, where $Q_i$ is the internal quality factor of the cavity. $b$ accounts for and adjusts the reference value of the transmission signal.


https://doi.org/10.1021/acs.nanolett.3c04990
Nano Lett. 2024, 24, 4369−4375

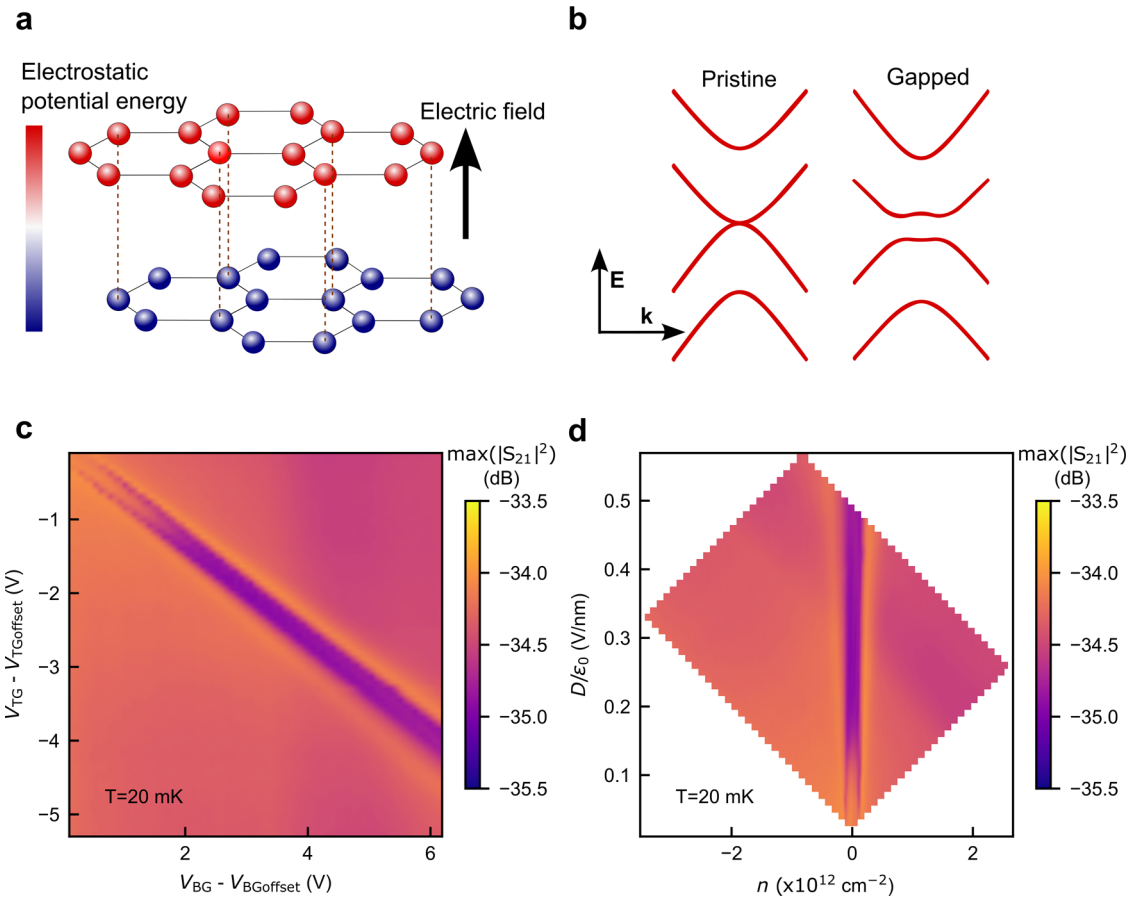


**Figure 3.** The transmitted signal through the cavity as a function of the gate voltages. (a) Upon applying a perpendicular displacement field, an electrostatic potential energy difference is created between the two layers of bilayer graphene, resulting in the breaking of inversion symmetry. (b) Left: The schematic shows that the pristine bilayer graphene has a zero band gap in its electronic structure. Right: Upon application of a perpendicular displacement field, a gap opens up due to the breaking of inversion symmetry. (c) For each ($V_{TG}$, $V_{BG}$), the transmitted signal through the cavity is measured as a function of frequency. The peak value of the amplitude of the transmission coefficient, max($|S_{21}|^2$) is plotted as a function of $V_{BG}$ and $V_{TG}$. There is a finite offset in both the $V_{BG}$ and $V_{TG}$ axes due to charge doping in BLG from the metallic gates. The measurements are done at 20 mK. (d) max($|S_{21}|^2$) is plotted as a function of $n$ and $D/\epsilon_0$. The region of low transmission along the displacement field corresponds to the opening of the band gap in BLG.

In Figure 4a, the resonant frequency, i.e., the frequency at which the amplitude of $S_{21}$ is maximum is plotted in the ($n$, $D/\epsilon_0$) plane. In Figure 4b, the frequency line-slice for two ($n$, $D/\epsilon_0$) points are shown. When the BLG has an opening in the gap, its resonant frequency shifts downward, and this frequency shift becomes more pronounced as the band gap increases.

For each ($n$, $D/\epsilon_0$), the $S_{21}$ frequency response is fitted using eq 1. To address the observed asymmetry in the frequency line-slice data caused by background effects, a skewness term $(1 + erf(s(f - f_0)))$ is multiplied with the fitting function, where $erf$ is the error function and $s$ is the skewness factor. The extracted capacitance value $C_2$ from the fitting is plotted in Figure 4c (for details of the fitting procedure, see Supporting Information, section 5). This capacitance value, which increases when a gap opens in the BLG, directly correlates with the DOS of BLG. Using our cavity-based technique, subfemtofarad change in capacitance can be measured accurately (see Supporting Information, Figure S6). The accuracy of our capacitance measurement has been compared with other state-of-the-art techniques[38,39] (see Supporting Information, section 7 for details).

The extracted capacitance $C_2$ represents the penetration field capacitance between the top gate and bottom gate, where grounded BLG screens the electric field due to its finite DOS.[39,47] By considering the BLG as an infinitely thin sheet, the expression for the measured capacitance can be written as[39]

$$C_2 = \frac{\epsilon_0 A_t d_g \epsilon_{hBN}^2}{d_g \epsilon_{hBN}(d_b + d_t) + \epsilon_0 d_b d_t} + C_S \quad (2)$$

Here $A_t$ is the area of the top gate covering the BLG; $d_b$ and $d_t$ are the thickness of the bottom hBN and top hBN, respectively; $\epsilon_{hBN}$ and $\epsilon_0$ are the permittivity of hBN and free space, respectively. $d_g = \frac{\epsilon_0}{e^2}\frac{\partial \mu}{\partial n}$ is the parametrization of $\frac{1}{e^2}\frac{\partial \mu}{\partial n}$ in units of length, where $\frac{\partial \mu}{\partial n}$ is the inverse DOS of the BLG. The inverse DOS is related to the electronic compressibility ($K$) as $K^{-1} = n^2\frac{\partial \mu}{\partial n}$. The stray capacitance $C_S$, assumed to be 47.81 fF, is estimated using the area of the top gate 110 $\mu m^2$ and the $d_t$ = 32.9 ± 0.6 nm and $d_b$ = 50.1 ± 1 nm. These thickness values have been measured using atomic force microscopy (AFM; see Supporting Information, section 6 for details). From eq 2 one can see that $C_2$ increases as the DOS decreases. In the pristine BLG, the DOS is high when there is no band gap in its electronic structure. As a result, BLG


https://doi.org/10.1021/acs.nanolett.3c04990
Nano Lett. 2024, 24, 4369−4375

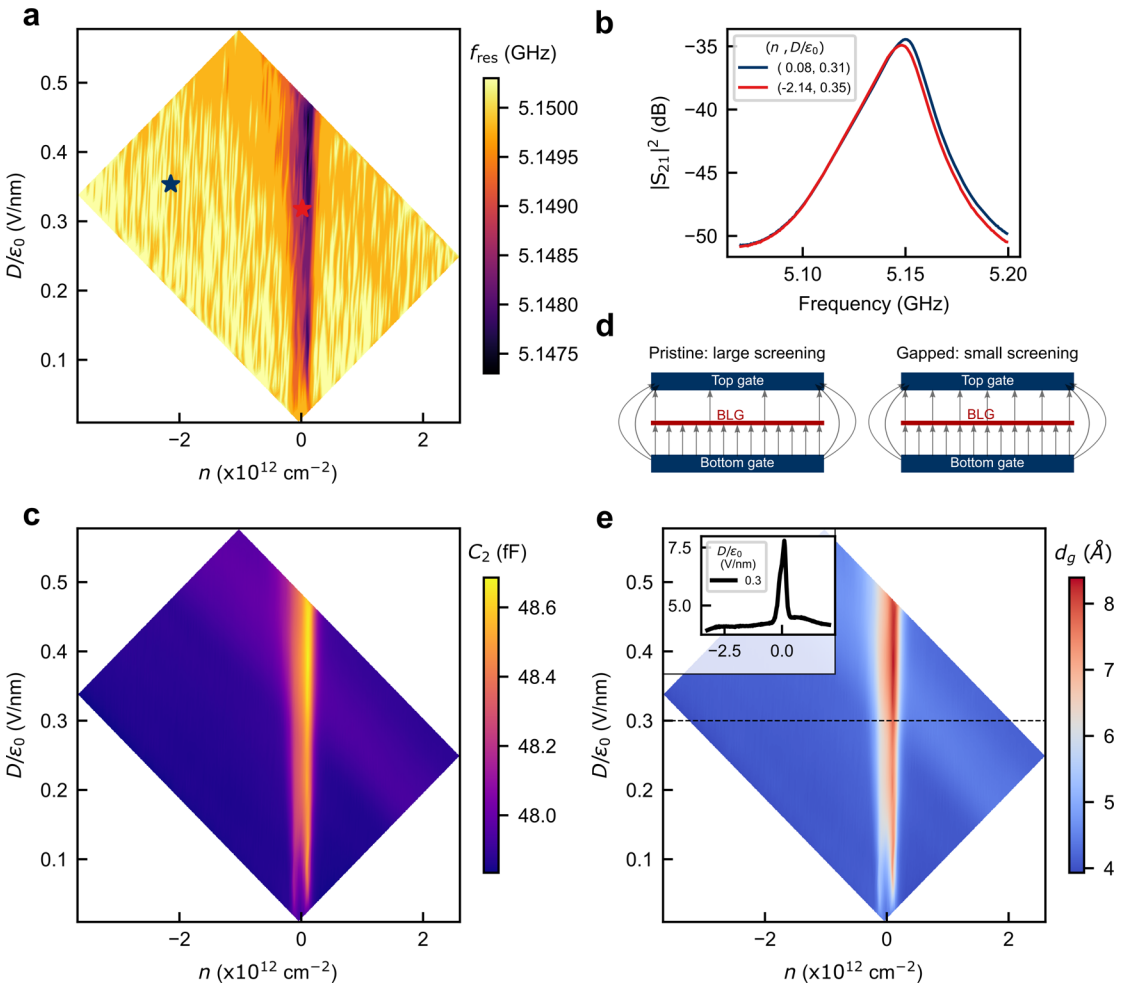


**Figure 4.** Measurement of the capacitance of the BLG heterostructure. (a) Shows the change in resonant frequency as a function of $n$ and $D/\epsilon_0$. The resonant frequency is shifting downward with the gap opening in BLG. (b) Shows the frequency line-slice at two ($n$, $D/\epsilon_0$) points as marked in panel (a). (c) Shows the extracted capacitance $C_2$ from the fitting as a function of $n$ and $D/\epsilon_0$. The capacitance increases with gap opening in the BLG, which is a consequence of the decreased density of states (DOS) of the BLG, which can also be interpreted from eq 2. (d) Left: In pristine BLG when there is no band gap in its electronic structure, the DOS of BLG is high. The BLG acts more like a metal in this regime, thus effectively screening the electric field between the top and bottom gates. Right: With a gap opening in BLG induced by a perpendicular displacement field, the DOS of BLG significantly decreases, transforming BLG into more of an insulator. Consequently, the screening effect is less prominent. (e) Shows the extracted $d_g$ from the panel (c) using eq 2, where $d_g$ is related to the inverse DOS ($\frac{1}{\epsilon^2}\frac{\partial\mu}{\partial n}$) of BLG as $d_g = \frac{\epsilon_0}{\epsilon^2}\frac{\partial\mu}{\partial n}$. The inset shows the line slice of $d_g$ with $n$ at $D/\epsilon_0$ = 0.3 V/nm.

screens the electric field between the top and bottom gates more effectively, resulting in a decrease in the $C_2$ (as depicted in Figure 4d). Upon application of a perpendicular displacement field, a gap opens in BLG, substantially reducing the DOS. Consequently, the screening is less effective for gapped BLG (as shown in Figure 4b) and $C_2$ increases.

From the extracted capacitance $C_2$, $d_g$ is obtained using eq 2 and is shown in Figure 4e. The value of $d_g$ matches well with previous reports.[39] The line slice of the extracted $d_g$ at $D/\epsilon_0$ = 0.3 V/nm is shown in the inset of Figure 4e. The $d_g$ has a sharp peak at $n$ = 0 and decreases asymmetrically on either side of $n$ = 0. The peak in $d_g$ can be interpreted as the emergence of a band gap in bilayer graphene (BLG), resulting in a reduced DOS. The data can be explained by a minimal tight-binding model of BLG. The inverse DOS has been calculated by solving the tight-binding Hamiltonian with a gap size Δ, which agrees well with the experimental data (see Supporting Information, section 8 for details).[48]

In summary, in this study, a half-wave SCPW cavity is used to characterize the electronic compressibility of BLG, establishing a direct correlation between the transmitted signal through the cavity and the band gap in the BLG as a function of the displacement field. Also, from the shift in resonant frequency, the capacitance of the stack is extracted, which directly correlates with the inverse DOS of the BLG. This noncontact microwave cavity-based technique provides a scope for noninvasive sensing of DOS in 2D materials.

Our methodology can be easily extended to the study of other 2D materials, as well. Furthermore, this technique holds promise for gaining insights into moiré superlattices of transition metal dichalcogenides, which have gained significant attention as a promising platform as a quantum simulator.[43] Importantly, our technique overcomes the challenge of contact resistance, which hampers the study of many exciting 2D materials. In addition, the choice of microwave frequencies will also enable fast dynamical measurements[10,13,40] in a cavity-coupled 2D van der Waals system.



https://doi.org/10.1021/acs.nanolett.3c04990
Nano Lett. 2024, 24, 4369−4375

## ■ ASSOCIATED CONTENT

### Supporting Information

The Supporting Information is available free of charge at https://pubs.acs.org/doi/10.1021/acs.nanolett.3c04990.

Device fabrication, measurement details, COMSOL simulation, additional data, fitting procedure, atomic force microscopy of the hBN flakes, comparison with other works, and density of states calculation of bilayer graphene (PDF)

## ■ AUTHOR INFORMATION


### Corresponding Author

**Mandar M. Deshmukh** − *Department of Condensed Matter Physics and Materials Science, Tata Institute of Fundamental Research, Mumbai 400005, India;* orcid.org/0000-0002-1401-1080; Email: deshmukh@tifr.res.in

### Authors

**Krishnendu Maji** − *Department of Condensed Matter Physics and Materials Science, Tata Institute of Fundamental Research, Mumbai 400005, India*

**Joydip Sarkar** − *Department of Condensed Matter Physics and Materials Science, Tata Institute of Fundamental Research, Mumbai 400005, India*

**Supriya Mandal** − *Department of Condensed Matter Physics and Materials Science, Tata Institute of Fundamental Research, Mumbai 400005, India*

**Sriram H.** − *Department of Condensed Matter Physics and Materials Science, Tata Institute of Fundamental Research, Mumbai 400005, India*

**Mahesh Hingankar** − *Department of Condensed Matter Physics and Materials Science, Tata Institute of Fundamental Research, Mumbai 400005, India*

**Ayshi Mukherjee** − *Department of Condensed Matter Physics and Materials Science, Tata Institute of Fundamental Research, Mumbai 400005, India*

**Soumyajit Samal** − *Department of Condensed Matter Physics and Materials Science, Tata Institute of Fundamental Research, Mumbai 400005, India*

**Anirban Bhattacharjee** − *Department of Condensed Matter Physics and Materials Science, Tata Institute of Fundamental Research, Mumbai 400005, India*

**Meghan P. Patankar** − *Department of Condensed Matter Physics and Materials Science, Tata Institute of Fundamental Research, Mumbai 400005, India*

**Kenji Watanabe** − *Research Center for Functional Materials, National Institute for Materials Science, Tsukuba 305-0044, Japan;* orcid.org/0000-0003-3701-8119

**Takashi Taniguchi** − *International Center for Materials Nanoarchitectonics, National Institute for Materials Science, Tsukuba 305-0044, Japan;* orcid.org/0000-0002-1467-3105

Complete contact information is available at: https://pubs.acs.org/10.1021/acs.nanolett.3c04990


### Notes

The authors declare no competing financial interest.

## ■ ACKNOWLEDGMENTS

We thank R. Vijay and V. Singh for their helpful discussions and comments. We thank H. Agarwal and D. Jangade for helping with device fabrication and S. Layek for helping with data analysis. We thank U. Ghorai for helping with the tight binding calculation. We acknowledge the Nanomission Grant SR/NM/NS-45/2016 and the DST SUPRA SPR/2019/001247 Grant, along with the Department of Atomic Energy of Government of India (12-R&D-TFR-5.10-0100) for support. We also acknowledge support from the Department of Science and Technology, India, via the QuEST Programme. M.M.D. acknowledges support from the J.C. Bose Fellowship JCB/2022/000045 from the Department of Science and Technology of India. Preparation of hBN single crystals were supported by the Elemental Strategy Initiative conducted by the Ministry of Education, Culture, Sports, Science and Technology, Japan (Grant Number JPMXP0112101001) and Japan Society for the Promotion of Science KAKENHI (Grant Numbers 19H05790 and JP20H00354).

## ■ REFERENCES


(1) Göppl, M.; Fragner, A.; Baur, M.; Bianchetti, R.; Filipp, S.; Fink, J. M.; Leek, P. J.; Puebla, G.; Steffen, L.; Wallraff, A. Coplanar waveguide resonators for circuit quantum electrodynamics. *J. Appl. Phys.* **2008**, *104*, 113904.

(2) Wallraff, A.; Schuster, D. I.; Blais, A.; Frunzio, L.; Huang, R.-S.; Majer, J.; Kumar, S.; Girvin, S. M.; Schoelkopf, R. J. Strong coupling of a single photon to a superconducting qubit using circuit quantum electrodynamics. *Nature* **2004**, *431*, 162−167.

(3) Wallraff, A.; Schuster, D. I.; Blais, A.; Frunzio, L.; Majer, J.; Devoret, M. H.; Girvin, S. M.; Schoelkopf, R. J. Approaching Unit Visibility for Control of a Superconducting Qubit with Dispersive Readout. *Phys. Rev. Lett.* **2005**, *95*, 060501.

(4) Schuster, D. I.; Houck, A. A.; Schreier, J. A.; Wallraff, A.; Gambetta, J. M.; Blais, A.; Frunzio, L.; Majer, J.; Johnson, B.; Devoret, M. H.; Girvin, S. M.; Schoelkopf, R. J. Resolving photon number states in a superconducting circuit. *Nature* **2007**, *445*, 515−518.

(5) Majer, J.; Chow, J. M.; Gambetta, J. M.; Koch, J.; Johnson, B. R.; Schreier, J. A.; Frunzio, L.; Schuster, D. I.; Houck, A. A.; Wallraff, A.; Blais, A.; Devoret, M. H.; Girvin, S. M.; Schoelkopf, R. J. Coupling superconducting qubits via a cavity bus. *Nature* **2007**, *449*, 443−447.

(6) Tholén, E. A.; Ergül, A.; Doherty, E. M.; Weber, F. M.; Grégis, F.; Haviland, D. B. Nonlinearities and parametric amplification in superconducting coplanar waveguide resonators. *Appl. Phys. Lett.* **2007**, *90*, 253509.

(7) Castellanos-Beltran, M. A.; Lehnert, K. W. Widely tunable parametric amplifier based on a superconducting quantum interference device array resonator. *Appl. Phys. Lett.* **2007**, *91*, 083509.

(8) Day, P. K.; LeDuc, H. G.; Mazin, B. A.; Vayonakis, A.; Zmuidzinas, J. A broadband superconducting detector suitable for use in large arrays. *Nature* **2003**, *425*, 817−821.

(9) Lee, G.-H.; Efetov, D. K.; Jung, W.; Ranzani, L.; Walsh, E. D.; Ohki, T. A.; Taniguchi, T.; Watanabe, K.; Kim, P.; Englund, D.; Fong, K. C. Graphene-based Josephson junction microwave bolometer. *Nature* **2020**, *586*, 42−46.

(10) Stehlik, J.; Liu, Y.-Y.; Quintana, C.; Eichler, C.; Hartke, T.; Petta, J. Fast Charge Sensing of a Cavity-Coupled Double Quantum Dot Using a Josephson Parametric Amplifier. *Physical Review Applied* **2015**, *4*, 014018.

(11) Hou, J. T.; Liu, L. Strong Coupling between Microwave Photons and Nanomagnet Magnons. *Phys. Rev. Lett.* **2019**, *123*, 107702.

(12) Mandal, S.; Kapoor, L. N.; Ghosh, S.; Jesudasan, J.; Manni, S.; Thamizhavel, A.; Raychaudhuri, P.; Singh, V.; Deshmukh, M. M. Coplanar cavity for strong coupling between photons and magnons in van der Waals antiferromagnet. *Appl. Phys. Lett.* **2020**, *117*, 263101.

(13) Amsüss, R.; Koller, C.; Nöbauer, T.; Putz, S.; Rotter, S.; Sandner, K.; Schneider, S.; Schramböck, M.; Steinhauser, G.; Ritsch, H.; Schmiedmayer, J.; Majer, J. Cavity QED with Magnetically Coupled Collective Spin States. *Phys. Rev. Lett.* **2011**, *107*, 060502.

(14) Kubo, Y.; Ong, F. R.; Bertet, P.; Vion, D.; Jacques, V.; Zheng, D.; Dréau, A.; Roch, J.-F.; Auffeves, A.; Jelezko, F.; Wrachtrup, J.; Barthe, M. F.; Bergonzo, P.; Esteve, D. Strong Coupling of a Spin Ensemble to a Superconducting Resonator. *Phys. Rev. Lett.* **2010**, *105*, 140502.
(15) Ranjan, V.; de Lange, G.; Schutjens, R.; Debelhoir, T.; Groen, J. P.; Szombati, D.; Thoen, D. J.; Klapwijk, T. M.; Hanson, R.; DiCarlo, L. Probing Dynamics of an Electron-Spin Ensemble via a Superconducting Resonator. *Phys. Rev. Lett.* **2013**, *110*, 067004.
(16) Regal, C. A.; Teufel, J. D.; Lehnert, K. W. Measuring nanomechanical motion with a microwave cavity interferometer. *Nat. Phys.* **2008**, *4*, 555−560.
(17) Singh, V.; Bosman, S. J.; Schneider, B. H.; Blanter, Y. M.; Castellanos-Gomez, A.; Steele, G. A. Optomechanical coupling between a multilayer graphene mechanical resonator and a superconducting microwave cavity. *Nat. Nanotechnol.* **2014**, *9*, 820−824.
(18) Sahu, S. K.; Mandal, S.; Ghosh, S.; Deshmukh, M. M.; Singh, V. Superconducting Vortex-Charge Measurement Using Cavity Electromechanics. *Nano Lett.* **2022**, *22*, 1665−1671.
(19) Schmidt, F. E.; Bothner, D.; Rodrigues, I. C.; Gely, M. F.; Jenkins, M. D.; Steele, G. A. Current Detection Using a Josephson Parametric Upconverter. *Physical Review Applied* **2020**, *14*, 024069.
(20) Endo, Y.; Onishi, M.; Muroga, S.; Arai, K.; Yanagi, K.; Shimada, Y.; Yamaguchi, M. GHz Range Magnetic Field Measurement of a Coplanar Waveguide with a Magnetic Force Microscope Tip by Exploiting a Beat Signal Between the Coplanar Waveguide and an Exciting Coil. *IEEE Trans. Magn.* **2014**, *50*, 1−4.
(21) de Visser, P. J.; Baselmans, J. J. A.; Bueno, J.; Llombart, N.; Klapwijk, T. M. Fluctuations in the electron system of a superconductor exposed to a photon flux. *Nat. Commun.* **2014**, *5*, 3130.
(22) Cao, Y.; Fatemi, V.; Demir, A.; Fang, S.; Tomarken, S. L.; Luo, J. Y.; Sanchez-Yamagishi, J. D.; Watanabe, K.; Taniguchi, T.; Kaxiras, E.; Ashoori, R. C.; Jarillo-Herrero, P. Correlated insulator behaviour at half-filling in magic-angle graphene superlattices. *Nature* **2018**, *556*, 80−84.
(23) Cao, Y.; Fatemi, V.; Fang, S.; Watanabe, K.; Taniguchi, T.; Kaxiras, E.; Jarillo-Herrero, P. Unconventional superconductivity in magic-angle graphene superlattices. *Nature* **2018**, *556*, 43−50.
(24) Ma, C.; Wang, Q.; Mills, S.; Chen, X.; Deng, B.; Yuan, S.; Li, C.; Watanabe, K.; Taniguchi, T.; Du, X.; Zhang, F.; Xia, F. Moiré Band Topology in Twisted Bilayer Graphene. *Nano Lett.* **2020**, *20*, 6076−6083.
(25) Pan, Y.; Fölsch, S.; Nie, Y.; Waters, D.; Lin, Y.-C.; Jariwala, B.; Zhang, K.; Cho, K.; Robinson, J. A.; Feenstra, R. M. Quantum-Confined Electronic States Arising from the Moiré Pattern of MoS2−WSe2 Heterobilayers. *Nano Lett.* **2018**, *18*, 1849−1855.
(26) Schoelkopf, R. J.; Wahlgren, P.; Kozhevnikov, A. A.; Delsing, P.; Prober, D. E. The Radio-Frequency Single-Electron Transistor (RF-SET): A Fast and Ultrasensitive Electrometer. *Science* **1998**, *280*, 1238−1242.
(27) Malinowski, F. K.; Han, L.; De Jong, D.; Wang, J.-Y.; Prosko, C. G.; Badawy, G.; Gazibegovic, S.; Liu, Y.; Krogstrup, P.; Bakkers, E. P.; Kouwenhoven, L. P.; Koski, J. V. Radio-Frequency C - V Measurements with Subattofarad Sensitivity. *Physical Review Applied* **2022**, *18*, 024032.
(28) Johmen, T.; Shinozaki, M.; Fujiwara, Y.; Aizawa, T.; Otsuka, T. Radio-Frequency Reflectometry in Bilayer Graphene Devices Utilizing Microscale Graphite Back-Gates. *Physical Review Applied* **2023**, *20*, 014035.
(29) Schmidt, F. E.; Jenkins, M. D.; Watanabe, K.; Taniguchi, T.; Steele, G. A. A ballistic graphene superconducting microwave circuit. *Nat. Commun.* **2018**, *9*, 4069.
(30) Dou, Z.; Wakamura, T.; Virtanen, P.; Wu, N.-J.; Deblock, R.; Autier-Laurent, S.; Watanabe, K.; Taniguchi, T.; Guéron, S.; Bouchiat, H.; Ferrier, M. Microwave photoassisted dissipation and supercurrent of a phase-biased graphene-superconductor ring. *Physical Review Research* **2021**, *3*, L032009.
(31) Haller, R.; Fülöp, G.; Indolese, D.; Ridderbos, J.; Kraft, R.; Cheung, L. Y.; Ungerer, J. H.; Watanabe, K.; Taniguchi, T.; Beckmann, D.; Danneau, R.; Virtanen, P.; Schönenberger, C. Phase-dependent microwave response of a graphene Josephson junction. *Physical Review Research* **2022**, *4*, 013198.
(32) Kroll, J. G.; Uilhoorn, W.; van der Enden, K. L.; de Jong, D.; Watanabe, K.; Taniguchi, T.; Goswami, S.; Cassidy, M. C.; Kouwenhoven, L. P. Magnetic field compatible circuit quantum electrodynamics with graphene Josephson junctions. *Nat. Commun.* **2018**, *9*, 4615.
(33) Kokkoniemi, R.; Girard, J.-P.; Hazra, D.; Laitinen, A.; Govenius, J.; Lake, R. E.; Sallinen, I.; Vesterinen, V.; Partanen, M.; Tan, J. Y.; Chan, K. W.; Tan, K. Y.; Hakonen, P.; Möttönen, M. Bolometer operating at the threshold for circuit quantum electrodynamics. *Nature* **2020**, *586*, 47−51.
(34) Sarkar, J.; Salunkhe, K. V.; Mandal, S.; Ghatak, S.; Marchawala, A. H.; Das, I.; Watanabe, K.; Taniguchi, T.; Vijay, R.; Deshmukh, M. M. Quantum-noise-limited microwave amplification using a graphene Josephson junction. *Nat. Nanotechnol.* **2022**, *17*, 1147−1152.
(35) Butseraen, G.; Ranadive, A.; Aparicio, N.; Rafsanjani Amin, K.; Juyal, A.; Esposito, M.; Watanabe, K.; Taniguchi, T.; Roch, N.; Lefloch, F.; Renard, J. A gate-tunable graphene Josephson parametric amplifier. *Nat. Nanotechnol.* **2022**, *17*, 1153−1158.
(36) Wang, J. I.-J.; et al. Coherent control of a hybrid superconducting circuit made with graphene-based van der Waals heterostructures. *Nat. Nanotechnol.* **2019**, *14*, 120−125.
(37) Zhang, Y.; Tang, T.-T.; Girit, C.; Hao, Z.; Martin, M. C.; Zettl, A.; Crommie, M. F.; Shen, Y. R.; Wang, F. Direct observation of a widely tunable bandgap in bilayer graphene. *Nature* **2009**, *459*, 820−823.
(38) Young, A. F.; Dean, C. R.; Meric, I.; Sorgenfrei, S.; Ren, H.; Watanabe, K.; Taniguchi, T.; Hone, J.; Shepard, K. L.; Kim, P. Electronic compressibility of layer-polarized bilayer graphene. *Phys. Rev. B* **2012**, *85*, 235458.
(39) Henriksen, E. A.; Eisenstein, J. P. Measurement of the electronic compressibility of bilayer graphene. *Phys. Rev. B* **2010**, *82*, 041412.
(40) Pirkkalainen, J.-M.; Cho, S. U.; Li, J.; Paraoanu, G. S.; Hakonen, P. J.; Sillanpää, M. A. Hybrid circuit cavity quantum electrodynamics with a micromechanical resonator. *Nature* **2013**, *494*, 211−215.
(41) Yoo, H. M.; Korkusinski, M.; Miravet, D.; Baldwin, K. W.; West, K.; Pfeiffer, L.; Hawrylak, P.; Ashoori, R. C. Time, momentum, and energy resolved pump-probe tunneling spectroscopy of two-dimensional electron systems. *Nat. Commun.* **2023**, *14*, 7440.
(42) Komissarov, I.; Holder, T.; Queiroz, R. The quantum geometric origin of capacitance in insulators. *arXiv:2306.08035 [cond-mat.mes-hall]* **2023**, na.
(43) Kennes, D. M.; Claassen, M.; Xian, L.; Georges, A.; Millis, A. J.; Hone, J.; Dean, C. R.; Basov, D. N.; Pasupathy, A. N.; Rubio, A. Moiré heterostructures as a condensed-matter quantum simulator. *Nat. Phys.* **2021**, *17*, 155−163.
(44) Mi, X.; Cady, J. V.; Zajac, D. M.; Stehlik, J.; Edge, L. F.; Petta, J. R. Circuit quantum electrodynamics architecture for gate-defined quantum dots in silicon. *Appl. Phys. Lett.* **2017**, *110*, 043502.
(45) Nouchi, R.; Saito, T.; Tanigaki, K. Determination of Carrier Type Doped from Metal Contacts to Graphene by Channel-Length-Dependent Shift of Charge Neutrality Points. *Applied Physics Express* **2011**, *4*, 035101.
(46) Chen, Q.-M.; Pfeiffer, M.; Partanen, M.; Fesquet, F.; Honasoge, K. E.; Kronowetter, F.; Nojiri, Y.; Renger, M.; Fedorov, K. G.; Marx, A.; Deppe, F.; Gross, R. Scattering coefficients of superconducting microwave resonators. I. Transfer matrix approach. *Phys. Rev. B* **2022**, *106*, 214505.
(47) Young, A. F.; Levitov, L. S. Capacitance of graphene bilayer as a probe of layer-specific properties. *Phys. Rev. B* **2011**, *84*, 085441.
(48) McCann, E.; Koshino, M. The electronic properties of bilayer graphene. *Rep. Prog. Phys.* **2013**, *76*, 056503.


https://doi.org/10.1021/acs.nanolett.3c04990
*Nano Lett.* 2024, 24, 4369−4375